# A NEW RAMAN SPECTROSCOPY BASED METHOD FOR MONITORING THE CRYSTALLINITY RATIO OF POLYETHYLENE TEREPHTHALATE

Mouad Bouita, Jean-Philippe Tinnes, Patrice Bourson, Marc Malfois, Marc Ponçot

# A NEW RAMAN SPECTROSCOPY BASED METHOD FOR MONITORING THE CRISTALLINITY RATIO OF POLYETHYLENE TEREPHTALATE

**Mouad Bouita[1], Jean-Philippe Tinnes[1], Patrice Bourson[2], Marc Malfois[3], Marc Ponçot[1,*]**

[1] Université de Lorraine, CNRS, IJL, F- 54000 Nancy, France

[2] Université de Lorraine, CentraleSupélec, LMOPS, F-57000 Metz, France

[3] ALBA Synchrotron, S- 08290 Barcelona, Spain

***Corresponding author: marc.ponçot@univ-lorraine.fr**

## ABSTRACT

Tracking the Raman scattering bands of polyethylene terephthalate (PET) during thermal heating has allowed to establish criteria for monitoring the crystallinity ratio within a few seconds. The existing criteria, based on Raman bands at 998 $cm^{-1}$ and at 1096 $cm^{-1}$, present certain disparities from the crystallinity ratio given by the total heat flow in differential scanning calorimetry (DSC). Based on the evolution of the Raman bands, a newfound method allowing the effective calculation of crystallinity ratio is proposed. For the same, the band at 1727 $cm^{-1}$, which is characteristic of the C=O carbonyl bonds of the ester group of PET is used. The new criterion, designated $r^{1727,2}$, was compared and validated by DSC and XRD. This novel approach also provides access to information on the various conformational states of the bonds under study, i.e. their proportions and positions with respect to the plane of the macromolecule aromatic rings. Evidently, this allows to reveal the characteristic thermal behavior of the PET microstructure such as the glass transition, crystallization and melting. This method can be useful for the close detection, quantification, understanding and tracing of the micromechanisms involved at the macromolecular conformations scale during thermal cycles.

**Key words**: Polyethylene terephthalate, Differential scanning calorimetry, WAXS, Macromolecular conformations, Crystallinity ratio.

# INTRODUCTION

Measurement of the crystallinity ratio of semi-crystalline polymers is usually performed using destructive methods such as DSC [1] and densitometry [2] or more sophisticated and non-destructive tests such as X-ray diffraction [3]and spectroscopic methods such as FTIR, Raman etc. [4,5]. Some experiments allow to follow the evolution of the polymer microstructure, during the deformation for example, understanding the involved mechanisms. In particular, tracking the crystallinity ratio during the manipulation requires short acquisition times. This kind of experiment therefore requires high energy light sources provided in synchrotrons which is not suitable for routine studies.

Spectroscopic techniques such as Raman spectroscopy, are non-destructive techniques that are capable of giving several structural information at short acquisition times [5]. In the last decades by the use of optical fibers, portable Raman spectrometers were developed. As a result, innovative coupling systems such as DSC/Raman [6] and mechanical test/Raman [7] which allow to acquire several information related to the evolution of the structure of materials collected in real time during thermal and mechanical tests could also be developed [8]. The detailed study of the Raman spectra, provide information which allows the tracking of several mechanisms that are a result of strain and temperature effects [9].

It should be noted that Raman spectroscopy is very sensitive to the conformational states of PET. These conformations have been linked to the different phases of semi-crystalline polymer [10]. The crystallization of PET is highly dependent on the conformational states of the macromolecule. There are three bonds involved, firstly the C-O bond between the terephthalic group and the ester group. This bond can be present in the '*gauche'* or '*trans'* conformation. Secondly, the C-C bond of the ethylenic segment, which can also be present in the '*gauche'* or '*trans'* conformation. And finally, the ester groups of the terephthalic acid unit where both '*trans'* and '*cis'* conformations are possible. The crystallization of PET can take place only if all conformations are '*trans'*[10–12].

Several authors have established criteria for the study of crystallinity, orientation of amorphous and crystalline phases and damage in the case of a range of polymers based only on Raman spectroscopy [13–15]. These criteria were validated by comparing them to results obtained by other techniques such as X-ray diffraction or infrared spectroscopy. However, the studies have shown that in the case of PET, the different crystallinity criteria established did

not report what was really happening in the polymer but gave a qualitative idea of this ratio [15,16].

The monitoring of low energy modes has been studied [17], and it was possible to follow the crystallinity and separate it from anisotropy using the bands at 60,75,130, and 170 $cm^{-1}$ for PET. On another hand, the monitoring of the band 1727 $cm^{-1}$ allowed to associate the change of its width at half height (FWHM) with the density of the material [18,19], and this gave a primary idea on the crystallinity ratio of the material as this one varies with the density. Monitoring the FWHM has been the focus of several subsequent studies evaluating important transition temperatures such as the glass transition, cold crystallization and melting at the time of a controlled heating [15,16,20]. Several vibrational bands were found to contain contributions from both the crystalline and amorphous phases, so their deconvolution gave an idea of the amount of the crystalline lamellae in the polymer [20–24]. This deconvolution also gives an idea of the conformations present in the material at the time of the measurement. Recently, a criterion for calculating the crystallinity ratio of PET has been established using the bands 1095 $cm^{-1}$ and 1118 $cm^{-1}$ (two bands that characterize the crystalline and amorphous phases, respectively) [15,16,20]. It was then noted that there is a significant variation in the crystallinity ratio of the polymer calculated by this criterion compared to the one given by DSC, and an index was proposed to follow more accurately the variation of the crystallinity ratio but this does not give in any case the exact value of the latter.

The subject of this study is to review in the case of PET the different criteria established, understand their limitations and then propose a new criterion to calculate a crystallinity ratio consistent with the results of the DSC and more likely to X-ray diffraction technique. The proposed method will enable us to use Raman spectroscopy instead of the destructive techniques which will shorten the approach time.

## MATERIALS AND METHODS

Polyethylene terephthalate was supplied by Goodfellow [25] and is used as-received without any pre-treatment. It is in the form of a 300x300 $mm^2$ plate and is 3mm thick. The polymer is in a transparent amorphous initial state, with a density of 1.3g/$cm^3$ and a specific heat of 1200J/K/kg. Experiments were conducted at the Jean Lamour Institute in Nancy and consisted of thermal tests performed with a TA Q200 calorimeter [26]. The samples are put in capsules without cover. This will allow to make in-situ Raman acquisitions, during a thermal cycle. This can be done by using a coupling system that acts as a lid on the capsule in a way that the

spectroscope probe is positioned directly above the sample [16,20]. The thermal cycle is performed with a heating ramp rate of 5K/min and ranging from 30 ˚C to 280 ˚C. The Raman spectrometer used is an RXN1-785 nm from Kaiser Optical Systems. The laser has a wavelength of 785 nm, a power of 400mW and an optical fiber that allows to delocalize the probe and link it directly to the DSC-Raman coupling system [20]. The acquisition parameters are taken in such a way as to have a minimal time of 30 s for a good signal/noise ratio. And so, this allowed to have a spectrum every 2.5 ˚C.

The DSC data are analyzed by the "TA Universal Analysis Software" and the Raman data are processed by a home-made program encoded on the numerical software Matlab®. The spectra were preprocessed by applying a Savitsky-Golay smoothing of window 3 and order 0 [27] and then subtracting the baseline using a Wavelet-based algorithm [28,29]. This will allow the isolation of the different Raman bands for the calculation of the different crystallinity criteria. It is important to normalize the acquired spectra using the PET normalization band which is the band at 633 $cm^{-1}$, a temperature-insensitive band [30]. A fitting procedure that consists of a three sub-bands deconvolution is applied. And because of the asymmetry of the band to be fitted, conditions on the sub-bands made it possible to respect this form: firstly, the condition on position [x(1)< x(2)< x(3)] ensures avoiding band over-runs. A second condition written as [A(1)< A(3)< A(2)] allows to keep the asymmetry of the primary band. A(i) is the intensity of the sub-band i and x(i) is its position. The mathematical form of the sub-bands is given and discussed further in the discussion part.

The modulated DSC (MDSC) was also performed to understand some mechanisms occurring during the heating: a heating ramp was carried out on the same material and under Heat-Iso Temperature Modulation (HITM) conditions [31,32]. The experimental parameters of the modulated DSC are a heating rate of 5K/min, a modulation period of 60 s and an amplitude of 0.796˚C [33].

Finally, in order to confirm our results, a time-resolved wide angle X-ray scattering (WAXS) experiments (ALBA, Bl-11 NCD Sweet, Barcelona, Spain) coupled to a Linkam calorimeter were performed[34]. The monochromatic beam was set at 12.4 keV. The diffraction patterns (Debye-Scherrer chamber) were recorded on a 2-D CDD plate detector (Rayonix LX255-HS) placed at 92 mm behind the sample (permitting to record in transmission mode all the Debye-Scherrer rings/halos). The Linkam device allowed to reproduce the heating ramp of 5K/min. The patterns were analyzed with Fit2D software, and for each, a 360˚ azimuthal integration was performed to get a texture independent diffractogram. The calculation of the crystallinity ratio was done with a home-made program encoded on the numerical software Matlab®. The

used method for the calculation of the crystallinity ratio is given in the supporting information.

## RESULTS AND DISCUSSION

The results of the DSC are shown in Figure 1. It highlights the evolution of the heat flow as a function of temperature at a heating rate of 5K/min. The crystallinity ratio calculated by the relation $\chi_c = \frac{\Delta Hm}{\Delta H_m^0}$ [1] is also reported, where ΔHm is obtained after integrating the heat flow and $\Delta Hm^0$ is equal to 140 J/g [35].

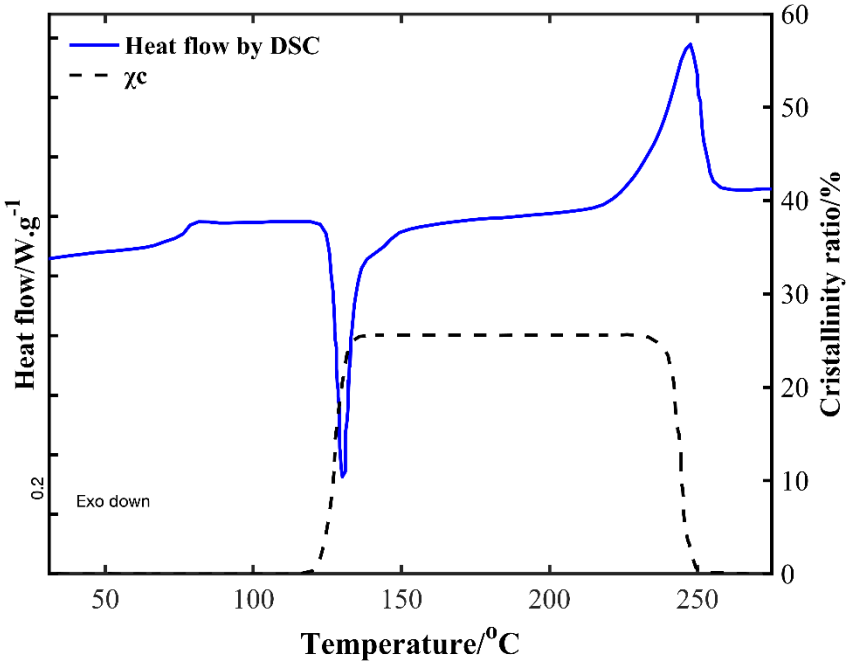


**Figure 1:** Evolutions of the heat flow and the crystallinity ratio for the initially amorphous PET during a heating ramp at 5K/min taking $\Delta Hm^0$ is equal to 140J/g.

In the case of amorphous PET, the crystallinity ratio remains constant and is equal to zero until the cold crystallization temperature (T=122˚C) is reached, and then rises to the value of 25 wt.%. The crystallinity ratio stays constant at this value until the first melting temperature (T=243,5˚C) is attained, thus bringing the degree of crystallinity back to its initial zero value at the totally molten state when the last melting temperature ($T_{m\ end}$=250 ˚C).

The processing of the previously acquired spectra is shown in Figure S1 (Supporting information). Some considerable changes are noticed especially at the time of cold crystallization and melting temperatures ranges.

The used zones for the calculation of the different criteria are highlighted using different colors.

The criteria to be studied will be denoted as $r^{998}$, $r^{1096,1}$, $r^{1096,2}$, $r^{1727,1}$ and are calculated using the following equations [20,36]:

$$\boldsymbol{r^{998} = I(998)} \quad (1)$$

$$\boldsymbol{r^{1096,1} = \frac{I(1096)}{I(1118)+I(1096)}} \quad (2)$$

$$\boldsymbol{r^{1096,2} = \frac{I(1096)-I(1096)a}{I(1118)+I(1096)}} \quad (3)$$

I(i) designate, here and after, the integral of the band i.

Lastly, the full width at half maximum (FWHM) of the band at 1727 $cm^{-1}$ allows to establish a criterion of densification and thus of crystallinity $r^{1727,1}$ by the following relations [18,19]:

$$\boldsymbol{r^{1727,1} = (\rho - \rho_a)/(\rho_c - \rho_a)} \quad (4)$$

$$\boldsymbol{\rho = (305 - \Delta\nu_{\frac{1}{2}})/209} \quad (5)$$

Where $\rho$ , $\rho_a$ and $\rho_c$ designate respectively the density of PET, its amorphous phase and its crystalline phase. Their values can be found in Ref [39,40].

Figure 2 shows the evolution of these four criteria applied to our PET during the first heating ramp performed in DSC compared to the crystallinity ratio $\chi_c$ calculated by DSC. Concerning $r^{998}$, and due to the difference between their values, both the crystallinity ratio and the area of the band at 998 $cm^{-1}$ are normalized by their maximum value and are reported in Figure 2.a. while the other criteria are reported in Figure 2.b.

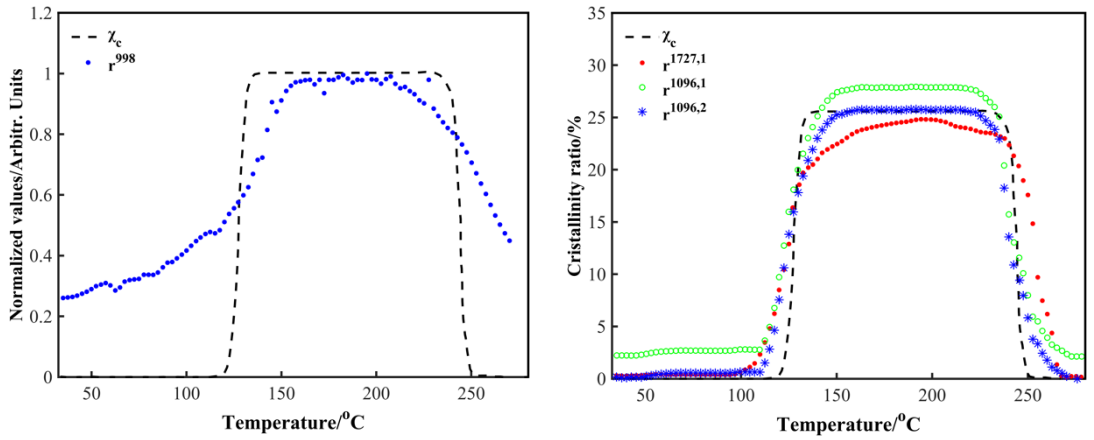


(a) (b)

**Figure 2:** Comparison between the crystallinity ratio and the crystallinity criteria (a) $r^{998}$ – (b) $r^{1096,1}$, $r^{1096,2}$ , $r^{1727,1}$ for the initially amorphous polyethylene terephthalate during a heating ramp at 5K/min.

The band at 998 $cm^{-1}$ characterizes the '*trans'* conformations of the C-C bond of the ethylene segment of PET [10,37]. According to Donnay, these conformations exist mainly in the crystalline phase (94%) [16]. We can notice an increase of this criterion then a decrease allowing to follow globally the crystallinity ratio. The criterion does not allow to follow effectively the crystallinity ratio brought by. This is justified by the fact that the band at 998 $cm^{-1}$ is directly related to the '*trans'* conformation of the C-C bond and not to the crystalline phase directly, the proportion of these conformations is then naturally greater than the zero value. This is indeed the case in the molten state as well as in the initial amorphous state. The increase in the criterion, before the cold crystallization temperature is explained by the '*gauche'* to '*trans'* conformation transition without any significant crystallization process [16]. This transition is only enhanced by the temperature. Additionally, this band has relatively low intensity compared to the overall spectrum. When it decreases in intensity, the measured area depends more and more on the noise of the signal which can be significant.

The second criterion $r^{1096,1}$ uses the areas of the two bands at 1096 $cm^{-1}$ and 1116 $cm^{-1}$. The 1096 $cm^{-1}$ band is characteristic of *'trans'* conformations of the C-O bond of the ethylene segment. The band at 1116 $cm^{-1}$ is often used as a normalization band for the '*gauche*' conformations of the same chemical bond [37]. The criterion thus represents the ratio of the '*trans'* conformations of the C-O bond and closely follows the evolution of the crystallinity ratio. In the crystallized state the value of the criterion considers the contribution of the '*trans*' conformations of the C-O bonds in the amorphous and crystalline phases [15,37]. This is evident from the value of the criterion in the molten and the initially amorphous states. The intensities are exactly the same confirming an equivalent average proportion in '*trans*' conformation in the amorphous phase.

The $r^{1096,2}$ criterion corrects this by subtracting from the previous one, the contribution of the '*trans*' conformations of the amorphous phase which will naturally be equal to the area of the vibration band at 1096 $cm^{-1}$ in the amorphous state (I(1096)a) [15]. However, there remains a non-negligible difference of this criterion with respect to the value of the DSC crystallinity ratio. It should also be noted that DSC measurements may also introduce some uncertainties at the time to choose the right baseline for the peaks area integration which may explain the differences between the proposed criteria and the DSC crystallinity values [1,38].

Concerning $r^{1727,1}$, the criterion can lead to inaccurate monitoring of crystallinity. Indeed, this criterion for the temperature range 122°C–245°C underestimates the degree of crystallinity while an overestimation out of this range is also observed.

The band at 1727 $cm^{-1}$ is characteristic of the C=O carbonyl bond of the ester group [18,24]. In order to promote crystallization, the bonds must be in '*trans*' conformation and in the plane of the aromatic ring [12]. The FWHM of the band at 1727 $cm^{-1}$ was strongly related to the density of the polymer [12,41]. Plotting its derivative in Figure S2 (Supporting information) gives a fairly accurate overview of the DSC thermogram. This makes it possible to identify the glass transition, the cold crystallization and the melting temperatures.

While tracking the 1727 $cm^{-1}$ band, it should be noted that a narrowing takes place before cold crystallization as shown in Figure S3 (Supporting information). After that, a broadening accompanied by an asymmetry happens at the melting and leads us to the same state as the amorphous initial state. This is explained by a conformational disorder of the out-of-plane rotational states of the carbonyl bonds in addition to the conformations of the ethylenic segment bonds in the amorphous phase [15,16,36]. The decrease in the width of the band is explained then by the resonance stabilization of the terephthatoyl group [36].

The asymmetry of the band at 1727 $cm^{-1}$ can be explained by the contribution of several bands. Those bands can highlight the presence and the contribution of the existing conformations [22–24]. Everall *et. al* [24] have therefore proposed a four-band deconvolution without giving much details about the physical meaning of the deconvolution. Many authors later have proven that the four-band deconvolution cannot be applied to such band [16,22,23]. This was also not retained in our case because it results in a rather broad residue. Following the example of Adar *and al* [22] we apply a three-band deconvolution located at 1717 $cm^{-1}$, 1726 $cm^{-1}$ and 1738 $cm^{-1}$ as shown in Figure 3.

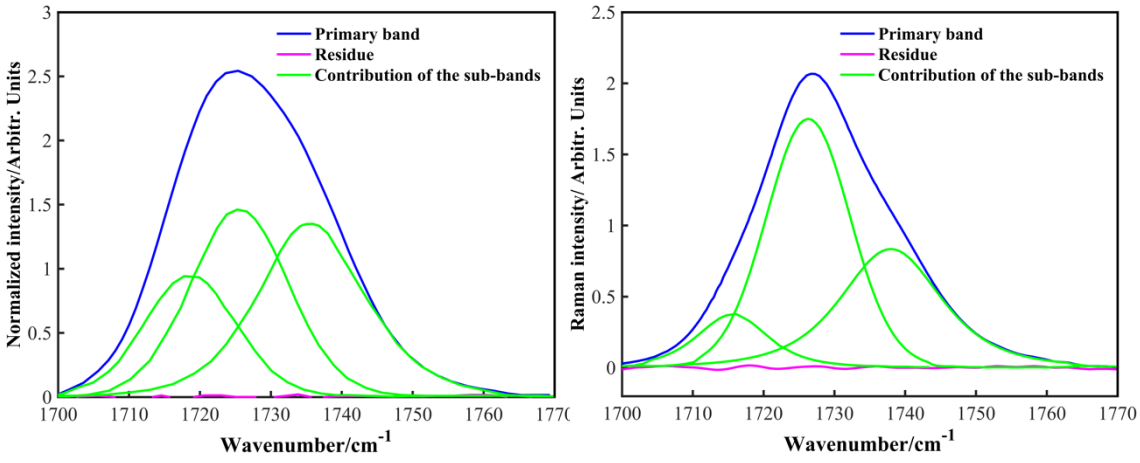


(a) (b)

**Figure 3:** Deconvolution of the 1727 $cm^{-1}$ band to three sub-bands at 1717 $cm^{-1}$, 1726 $cm^{-1}$ and 1738 $cm^{-1}$ in the amorphous and semi-crystallized state of PET at (a)- T=30˚C, (b)- T=150 ˚C.

As a first step, it was chosen to use a mathematical function which is the so-called Pearson VII function with the following formula:

$$f(x) = \left[1 + \left(\frac{2.(x-x_0).\sqrt{2^{1/M}-1}}{w}\right)^2\right]^{-M} \quad (6)$$

where M is the form factor of the function and depending on its value, the function can be either Gaussian (M>>8) or Lorentz (M<1), otherwise it can be approximated to a Pseudo-Voigt.

For a first approach, no condition is set on the parameter M.

The evolution of the form factors in Figure 4 allows the mathematical shape of the bands to be determined and are therefore summarized as the following:

1717 $cm^{-1}$: Gaussian.
1726 $cm^{-1}$: Gaussian.
1738 $cm^{-1}$: Pseudo Voigt.

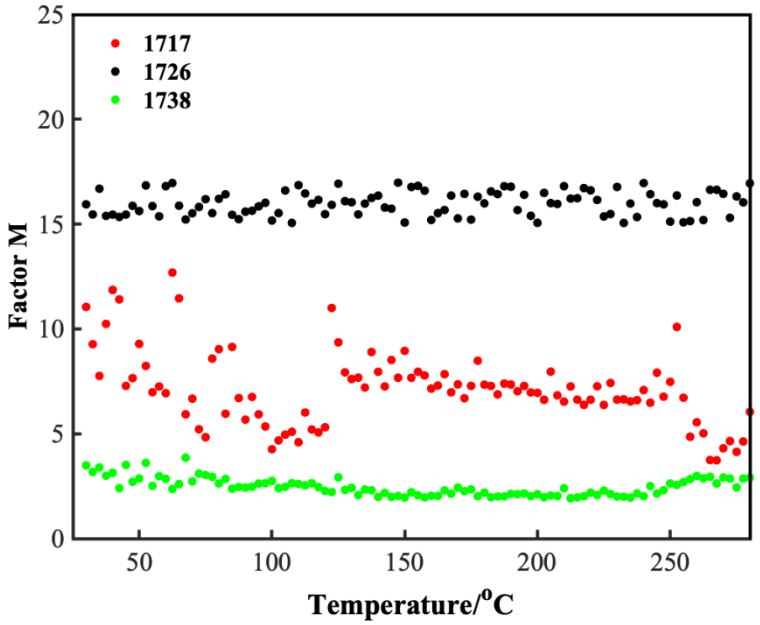


**Figure 4**: Evolution of the factor form M of the three sub-bands during a heating ramp at 5K/min for an initially amorphous PET.

The evolution of the proportions of areas of these three sub-bands is reported in Figure 5 It is easily observed that the three proportions vary with the crystallinity ratio. The two bands at 1738 $cm^{-1}$ and 1726 $cm^{-1}$ have approximately the same contributions below the cold

crystallization temperature and above the melting temperatures. Between these two thermal events, the two bands at 1738 $cm^{-1}$ and 1717 $cm^{-1}$ see their contributions decrease in favor of the central band.

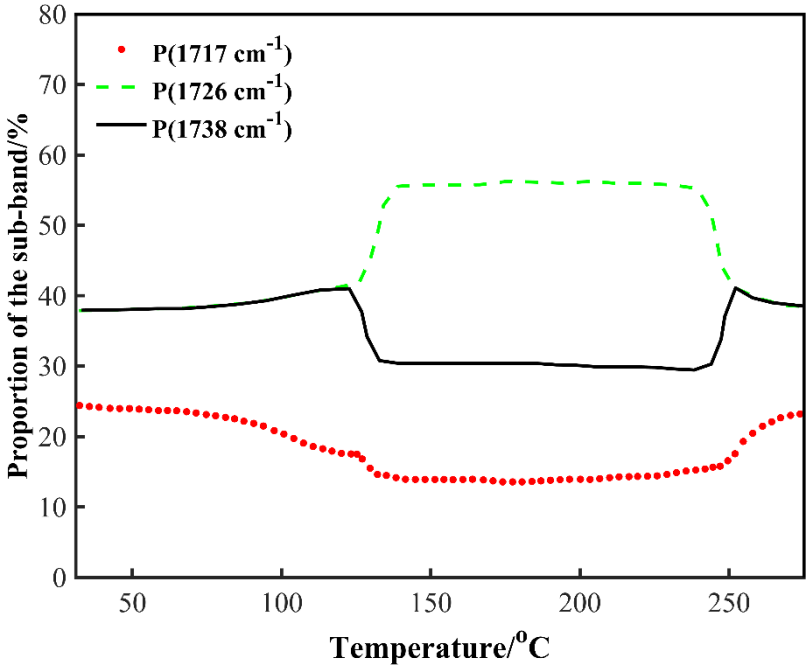


**Figure 5:** Evolution of the proportions of areas of the three bands at 1717 $cm^{-1}$,1726 $cm^{-1}$ and 1738 $cm^{-1}$.

The criterion $r^{1727,2} = \frac{I(1726)-I(1738)}{I_{tot}}$ (6) plotted in Figure 6 allows to track the change in crystallinity ratio given by DSC very accurately. $I_{tot}$ is the sum of areas limited by the three sub-bands. As previously discussed, the crystalline phase is favored by C=O bonds in the plane of the '*trans'* aromatic ring. The amorphous phase is described as randomly out-of-plane bonds in an aromatic ring. Band allocation can be suggested as follows:

1726 $cm^{-1}$: '*trans*' conformations in all planes.

1738 $cm^{-1}$: '*trans*' conformations outside the aromatic plane.

1717 $cm^{-1}$: off '*trans*' conformations or '*cis*' conformations, more accurately.

Thus, the criterion represents the proportion of '*trans*' conformations of the C=O bonds in the aromatic plane. These suggestions are also supported by the mathematical form of the sub-bands. Indeed, the sub-band at 1726 $cm^{-1}$ which characterizes '*trans*' conformations in all planes must have a Gaussian character due to the fact that these conformations are scattered throughout space. The sub-band at 1738 $cm^{-1}$ corresponds to '*trans*' conformations outside the plane. This remains in the Gaussian range but tends towards a Lorentz by the suppression

of the '*trans*' population in the aromatic plane, resulting in a lower M value than at 1726 $cm^{-1}$. It can also be characterized by a Pseudo-Voigt function with a Lorentz factor η= 0.2.
The band at 1717 $cm^{-1}$ also has a Gaussian character and corresponds to '*cis*' conformations.

The glass transition can also be highlighted by the slight change in the evolution of the three sub-band proportions around 80˚C, especially for the band at 1727 $cm^{-1}$. This is due to the initiation of the macromolecular mobility and the beginning of conformation transitions. These modifications will be more evident at the cold crystallization and the melting temperatures. However, a significant difference between the criterion and $\chi_c$ takes place in the melting zone. This fact can be explained by performing a modulated DSC experiment. The modulated DSC thermograms in Figure S4 (Supporting information), show that the total heat flow can be divided into two independent heat flow called reversing and non-reversing according to the following equation [31–33].

$$\frac{dH}{dt} = C_p \frac{dT}{dt} + f(T,t) \quad (7)$$

where $\frac{dH}{dt}$ is the total heat flow equivalent to a standard DSC experiment at the same average heating rate, $C_p \frac{dT}{dt}$ is usually called the reversing heat flow component and f(T,t) is the kinetic or the non-reversible component of the total heat flow and is calculated from the difference between the overall signal and the heat capacity component.

This result makes it possible to differentiate the different physical phenomena that take place during the heating ramp. On the reversing heat flow, the glass transition takes place at exactly T=79 °C, and melting at a temperature T=247 °C. Following the non-reversing flow, cold crystallization does takes place at T= 122 °C. Two important events also occur: the enthalpic recovery and the crystalline improvement [33,42,43]. The latter represents the process of crystals melting at temperatures below the thermodynamic melting point and then crystallizing and melting one or more times with temperature increasing. In the case where crystalline improvement is not considered in the calculation of the crystallinity ratio by DSC ($\chi_c$ modified), the difference between this crystallinity ratio and the $r^{1727,2}$ criterion is greatly reduced as shown in Figure 6. The previous discussion allowed us to understand that the criterion put in place is independent of crystalline perfection. The transitions that occur in this phenomenon does not affect the C=O double bond. The physical explanation of this finding is that during heating, and around the melting point, the melting in the crystalline improvement does not change the states of conformation. the bonds keep the conformations of the

crystalline state in their amorphous state. Involving a fast recrystallization which will disappear right after by melting. this phenomenon will be redundant until there is a radical change in the conformations present in the material. The criterion $r^{1727,2}$ is therefore sensitive to a cumulative degree of crystallinity. This means that any phenomenon that does not involve changes in the conformation states (e.g the crystalline improvement) will not affect the value of the criterion.

In order to validate the criterion, XRD experiments were performed. After the treatment of the 2D patterns, the evolution of the diffractograms during the heating ramp can be plotted in Figure S5 (Supporting information). Based on those diffractograms, one can get the crystallinity ratio by following the procedure mentioned in the supplementary material. Figure 6 shows also the comparison between $r^{1727,2}$ and XRD crystallinity ratio.

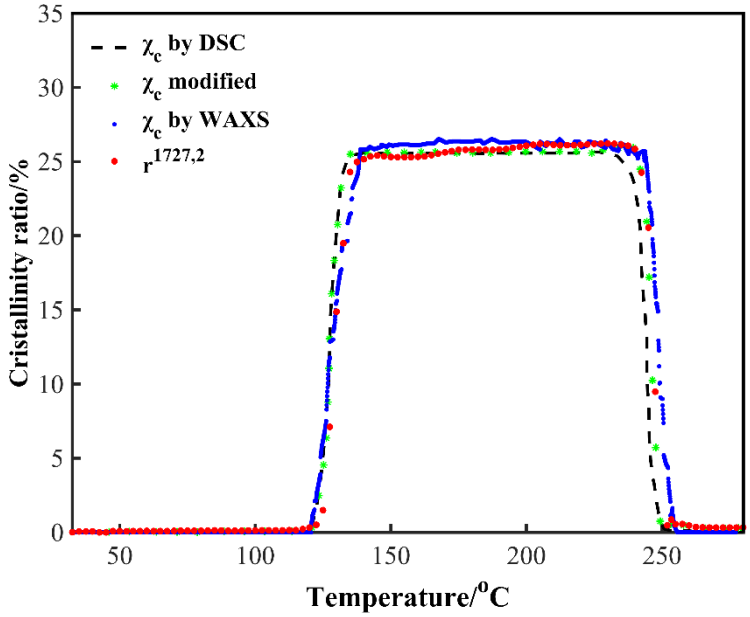


**Figure 6:** Comparison between the XRD, DSC and modified-DSC crystallinity ratios and the $r^{1727,2}$ criterion during a heating ramp at 5K/min for an initially amorphous PET.

Similar evolutions are observable. Nevertheless, a slight difference mainly located at the maximum value of the crystallinity ratio reached close to 140˚C highlights the greater precision of the Raman criterion compared to the XRD criterion at the time of the crystallization of the smallest lamellae for which the strict condition of having only '*trans*' conformations in the plane of the aromatic ring is not fully respected. Comparing the diffractograms at T=180˚C and T=240˚C in Figure S6 (Supporting information), the general narrowing of the crystalline peaks can be observed simultaneously to the drop of the crystallinity ratio. These modifications in their shape can be justified by a crystalline lamellae

perfecting process. This observation comes to support the fact that the criterion $r^{1727,2}$ does not take into account the crystalline perfection improvement as there is a slight difference between the WAXS and Raman crystallinity ratios until 200˚C.

# CONCLUSION

This study provides an accurate overview of the various crystallinity criteria presented in the literature using Raman spectroscopy measurements. For this purpose, a DSC/Raman coupling system has been developed. The comparison between the existing criteria and the crystallinity ratio obtained from DSC showed that the $r^{998}$ criterion is related to the '*trans'* conformations of the C-C bond in the ethylic segment and not to the crystalline part specifically and thus is not a precise criterion.

The $r^{1096,2}$ criterion is more precise and can monitor the crystallinity ratio but has been found to be unsuitable for *in situ* measurements during a tensile test [20].

Considering the differences between the established criteria and the crystallinity ratio obtained from DSC, a new approach has been developed to better determine the degree of crystallinity. This approach is based on the contribution of the various morphological configurations present in the material. The new criterion, designated $r^{1727,2}$, was compared and validated by DSC and XRD. It represents the amount of '*trans*' conformations of the C=O bond in the plane of the aromatic core. It gives access to a cumulative crystallinity rate.

This new method that allows monitoring of the crystallinity ratio, is based on the contribution of the different conformational configurations present in the material. This gives an idea on the effects of rotation of the macromolecular chains with respect to the plane of the aromatic core, the possible stabilization of the bonds and finally, more generally, the effect of the thermal transitions such as crystallization or fusion on the state of the conformations in general.

The suggested criterion, as it stands, may have the potential advantage of being independent of macromolecular orientation. And therefore, can accurately monitor the crystallinity during a tensile test.

Therefore, we can conclude that Raman spectroscopy can provide accurate information to identify and track in situ micro mechanisms that occur with temperature changes and why not when an external load is applied.

**ACKNOWLEDGEMENTS:** The authors wish to thank the LMOPS laboratory for their technical assistance and invaluable help during experiments. They also acknowledge the ALBA synchrotron for giving the opportunity to perform *in situ* XRD experiments.

## References

[1] P. Gill, T. T. Moghadam, B. Ranjbar, *J. Biomol. Tech.* **2010**, *21*, 167.
[2] J.-F. Pilichowski, T. Liptaj, M. Morel, E. Terriac, M. Baba, *Polym. Int.* **2003**, *52*, 1913.
[3] Kakudo Masao, *X-ray diffraction by polymers / Masao Kakudo,... Nobutami Kasai,...*, Kodansha Elsevier, Tokyo Amsterdam New York (N. Y.), **1972**.
[4] A. Käppler, F. Windrich, M. G. J. Löder, M. Malanin, D. Fischer, M. Labrenz, K.-J. Eichhorn, B. Voit, *Anal. Bioanal. Chem.* **2015**, *407*, 6791.
[5] B. H. Stuart, *Vib. Spectrosc.* **1996**, *10*, 79.
[6] T. Suzuki, K. Takahashi, H. Uehara, T. Yamanobe, *J. Therm. Anal. Calorim.* **2013**, *113*, 1543.
[7] J. Martin, M. Ponçot, J. M. Hiver, P. Bourson, A. Dahoun, *J. Raman Spectrosc* **2013**, 44, 776-784.
[8] M. Donnay, M. Ponçot, J.-P. Tinnes, T. Schenk, O. Ferry, I. Royaud, *Polym. Guilford* **2017**, *117*, 268.
[9] M. Ponçot, S. Chaudemanche, J. Martin, O. Ferry, T. Schenk, J.P. Tinnes, D. Chapron, I. Royaud, P. Bourson, A. Dahoun, *Polymer* **2015,** 80, 27-37.
[10] J. Štokr, P. Sedláček, D. Doskočilová, B. Schneider, J. Lövy, *Collect. Czechoslov. Chem. Commun.* **1981**, *46*, 1658.
[11] J. Štokr, B. Schneider, D. Doskočilová, J. Lövy, P. Sedláček, *Polymer* **1982**, *23*, 714.
[12] P. Sedláček, J. Štokr, B. Schneider, *Collect. Czechoslov. Chem. Commun.* **1981**, *46*, 1646.
[13] J. Martin, Etude par spectroscopie Raman du polypropylène isotactique au cours de sa déformation uniaxiale. These de doctorat, Université de Lorraine**, 2009.** https://www.theses.fr/2009METZ021S (accessed 9 June 2022).
[14] S. Chaudemanche, M. Ponçot, S. Andre, A. Dahoun, P. Bourson, *J. Raman Spectrosc* **2014,** 45, 369-376.
[15] K. B. Hafsia, M. Ponçot, D. Chapron, I. Royaud, A. Dahoun, P. Bourson, *J. Polym. Res.* **2016**, *23*, 1.
[16] M. Donnay, Étude des mécanismes de déformation de membranes polymères poreuses pour applications biomédicales, These de doctorat, Université de Lorraine, **2017,** https://www.theses.fr/2017LORR0228, (Confidential).
[17] P. Colomban, J.-M. Herrera-Ramirez, R. Paquin, A. Marcellan, A. R. Bunsell, *Eng. Fract. Mech.* **2006**, *73*, 2463.
[18] M. Richard-Lacroix, C. Pellerin, *Macromolecules* **2012**, *45*, 1946.
[19] A. J. Melveger, *J. Polym. Sci. Part -2 Polym. Phys.* **1972**, *10*, 317.
[20] K. B. Hafsia, Identification des micro-mécanismes de déformation du PET amorphe et semi-cristallin in situ au cours d'un essai mécanique, phdthesis, Université de Lorraine, **2016**. https://www.theses.fr/2016LORR0081 (accessed 9 June 2022).
[21] F. Adar, H. D. Noether, (Ed: W. G. Golden), Los Angeles, CA, **1992**, p. 42.
[22] F. Adar, H. Noether, *Polym. Guilford* **1985**, *26*, 1935.

[23] C. C. C. Lesko, J. F. Rabolt, R. M. Ikeda, B. Chase, A. Kennedy, *J. Mol. Struct.* **2000**, *521*, 127.
[24] N. Everall, P. Tayler, J. M. Chalmers, D. MacKerron, R. Ferwerda, J. H. van der Maas, *Polym. Guilford* **1994**, *35*, 3184.
[25] Polyester, PET, PETP Sheet - Polyethylene terephthalate (ES30-SH-000130), https://www.goodfellow.com/fr/fr/displayitemdetails/p/es30-sh-000130/polyethylene-terephthalate-sheet, (accessed 8 June 2022).
[26] G. Höhne, *Differential Scanning Calorimetry*, Springer Berlin Heidelberg, Berlin, Heidelberg, 2nd ed. 2003., **2003**.
[27] An Adaptive Savitsky-Golay Filter for Smoothing Finite Element Computation https://ulysse.univlorraine.fr/discovery/fulldisplay/cdi_arxiv_primary_1911_00790/33UDL_INST:UDL, (accessed 9 June 2022).
[28] F. Qian, Y. Wu, P. Hao, *Opt. Laser Technol.* **2017**, *96*, 202.
[29] LI XUELIANG, CHEN ZHENCHENG, XIA JINHONG, ZHU JIANMING, **2013**.
[30] O. S. Fleming, K. L. A. Chan, S. G. Kazarian, *Vib. Spectrosc.* **2004**, *35*, 3.
[31] M. Reading, D. J. Hourston, *Modulated Temperature Differential Scanning Calorimetry Theoretical and Practical Applications in Polymer Characterisation*, Springer Netherlands, Dordrecht, 1st ed. 2006., **2006**.
[32] L. C. Thomas, T. Instruments, L. Drive, N. Castle, 10. https://www.tainstruments.com/pdf/literature/TP_006_MDSC_num_1_MDSC.pdf (accessed 9 June 2022)
[33] L. C. Thomas, T. Instruments, L. Drive, N. Castle, 9. https://www.tainstruments.com/pdf/literature/TP_007_MDSC_num_1_MDSC.pdf (accessed 9 June 2022)
[34] S. Saidi, G. Portale, W. Bras, A. Longo, J. M. Amigo, D. Chapron, P. Bourson, D. Hermida-Merino, *Polymers* **2021**, *13*, 4203.
[35] A. Mehta, U. Gaur, B. Wunderlich, *J. Polym. Sci. Polym. Phys. Ed.* **1978**, *16*, 289.
[36] J. S. Kim, M. Lewin, B. J. Bulkin, *J. Polym. Sci. Part B Polym. Phys.* **1986**, *24*, 1783.
[37] F. J. Boerio, S. K. Bahl, *Spectrochim. Acta Part Mol. Spectrosc.* **1976**, *32*, 987.
[38] Y. P. Khanna, W. P. Kuhn, *J. Polym. Sci. Part B Polym. Phys.* **1997**, *35*, 2219.
[39] R. D. P. Daubeny, C. W. Bunn, C. J. Brown, *Proc. R. Soc. Lond. Ser. Math. Phys. Sci.* **1954**, *226*, 531.
[40] Y. Tomashpol'skii, G. S. Markova, *Polym. Sci. USSR* **1964**, *6*, 316.
[41] L. Song, W. Ma, Y. Ren, W. Zhou, S. Xie, P. Tan, L. Sun, *Appl. Phys. Lett.* **2008**, *92*, 121905.
[42] F. Fontaine, J. Ledent, G. Groeninckx, H. Reynaers, *Polymer* **1982**, *23*, 185.
[43] Y. P. Koh, S. L. Simon, *Macromolecules* **2013**, *46*, 5815.